Soils and Rocks
www.soilsandrocks.com
An International Journal of Geotechnical and Geoenvironmental Engineering
ISSN 1980-9743
ISSN-e 2675-5475

Numerical simulations of displacement piles in a tropical soil

Bismarck Chaussê Oliveira[1#], Maurício Martines Sales[1], Renato Resende Angelim[1], Luiz Carlos Galvani Junior[2]

Article

Keywords
Full-displacement piles
Finite element method
Installation effects of piles
Tropical soils
Lateritic soil
Deep foundations

Abstract

The behavior of pile foundations under axial loading is directly influenced by the effects that its installation process induces in the surrounding soil. Consequently, the consideration of these effects is essential for the correct numerical modeling of these geotechnical structures. In the present study, numerical simulations of driven cast-in-situ piles under axial loading have been carried out using finite element analysis. Three 3.5 m long piles with diameters ranging from 114.3 to 219.1 mm were analyzed. The pile installation effects have been considered indirectly by employing two distinct approaches, both based on the concepts of cylindrical cavity expansion. The behavior of the tropical soil profile is described with the Hardening Soil constitutive model. The load-displacement response and load distribution along the pile obtained with the numerical simulations have been analyzed and compared with in-situ load tests results. In the failure conditions, both approaches accurately predicted the bearing capacity of the piles, with an average error of only 2% compared to the measured values. The results in terms of load distribution over depth were also satisfactory. The difference between measured and numerical ultimate base resistance values ranged from 0% to 30%. The good agreement between the numerical and experimental results indicates that the proposed numerical approaches have been effective in simulating the piles installation process and reinforces the importance of considering the installation effects in the numerical modeling of these geotechnical structures. Both approaches can also be used to predict the bearing capacity of displacement piles.

1. Introduction

Pile foundations can be classified according to different criteria. Considering the induced changes in the density and stress state of the surrounding soil during the installation process, it is possible to categorize pile foundations into three groups: non-displacement piles, partial displacement piles, and full-displacement piles. Non-displacement piles installation usually results in a reduction in the density and stress state of the surrounding soil, while installation technologies of partial and full-displacement piles tend to increase such values proportionally to the magnitude of the induced displacement. Particularities in observed behavior depend on factors such as type of pile, installation technology, and soil type. These installation effects directly influence the mechanical response of the piles when subjected to external loads.

Driven cast-in-situ (DCIS) piles are a type of deep foundation classified as full-displacement piles due to their installation technology, but they have some similar aspects to non-displacement piles, such as in-situ casting of concrete and the resulting rough shaft interface (Flynn & McCabe, 2016).

Over the past few decades, numerical methods have been increasingly employed in the solution of engineering problems. When it comes to pile performance, the accuracy of numerical analyses is dependent on the pile modeling steps being representative of the pile installation technology and the soil constitutive model parameters being properly calibrated. While in the analysis of non-displacement piles installation effects can often be ignored without major losses in simulation accuracy (Wehnert & Vermeer, 2004), in the analysis of full-displacement piles, the consideration of these effects is essential.

Given the nature of the problem, numerical methods with formulations capable of analyzing large deformations problems are the most suitable for modeling full-displacement piles. Several researches have been done on this subject, using the discrete element method (Li et al., 2021; Lobo-Guerrero & Vallejo, 2005), the material point method (Lorenzo et al., 2018; Phuong et al., 2016; Tehrani et al., 2016) the arbitrary Lagrangian-Eulerian method (Rooz & Hamidi, 2019; Yang et al., 2020) and the coupled Eulerian-Lagrangian method (Heins & Grabe, 2017; Pucker & Grabe, 2012; Qiu et al., 2011).

#Corresponding author. E-mail address: bismarckchausse@gmail.com.
[1]Universidade Federal de Goiás, Escola de Engenharia Civil e Ambiental, Goiânia, GO, Brasil.
[2]SETE Engenharia, Goiânia, GO, Brasil.

Submitted on May 3, 2022; Final Acceptance on December 6, 2022; Discussion open until May 31, 2023.
https://doi.org/10.28927/SR.2023.004522

The standard finite element method (FEM), which uses Lagrangian formulation, has limitations in simulating large deformation problems due to distortions of the finite element mesh, which result in inaccurate or diverging solutions (Engin et al., 2015). Even when using remeshing after each calculation step (updated Lagrangian formulation), direct simulation of full-displacement pile installation processes can result in numerical problems due to the remapping of the state variables (Engin, 2013), and it is necessary to resort to modeling strategies that allow considering the installation of these geotechnical structures in an idealized way.

Several studies use varied numerical approaches to incorporate the installation effects of full-displacement piles indirectly via standard FEM (Broere & van Tol, 2006; Engin et al., 2015; Said et al., 2009) and using the updated mesh option (Krasinski, 2014; Rezania et al., 2017; Schmüdderich et al., 2020). However, there are still few works on this subject evaluating DCIS piles, especially those installed in heterogeneous tropical soil profiles.

This paper proposes adaptations to two different numerical approaches based on the concepts of cylindrical cavity expansion to simulate the installation of DCIS piles installed in a tropical soil profile. The approaches emphasize incorporating changes in the density and stress state of the soil surrounding the pile caused by the installation processes. The analyses are conducted in Plaxis 2D® finite element software (Brinkgreve et al., 2021) and the updated mesh option is used in some steps. The suitability of the approaches is attested by the agreement between numerical and experimental results, the latter obtained from in-situ static load tests.

2. Pile testing program

2.1 Geotechnical characterization of the tropical soil profile of the experimental field

The piles analyzed in this paper were installed in the Experimental Field of the School of Civil and Environmental Engineering of the Federal University of Goiás, located in Goiânia, a city in the state of Goiás, in the Center-West region of Brazil. The climatic conditions of the region favor the pedogenetic evolution and an intense chemical weathering that originate lateritic soils, whose mineralogical constitution is mainly composed of quartz, kaolinite, and iron/aluminum oxides and hydroxides. Among the main characteristics of these soils are high porosity, high permeability, high strength when compacted, and the presence of clay particle aggregates (Camapum de Carvalho & Gitirana Junior, 2021; Freitas et al., 2020).

According to the geotechnical characterization performed by Nascimento (2019) and Machado et al. (2020) (Figure 1), using MCT classification (Nogami & Villibor, 1995), the soil profile of the experimental field is composed of lateritic clayey sand (LA'-LG'), apparently transported, up to a depth of 4 m. The layer between 4 and 7 m depth seems to be a transition horizon, with a higher content of gravel in the middle of the layer. From 7 m depth on, the soil is no longer lateritic, and its clay content decreases, suggesting the beginning of the residual (saprolite) horizon. The values determined of specific gravity (G_s), unit weight of moist soil (γ), and void ratio (e) are typical of tropical soils. The percentages of the clay fraction in the grain size distributions with and without

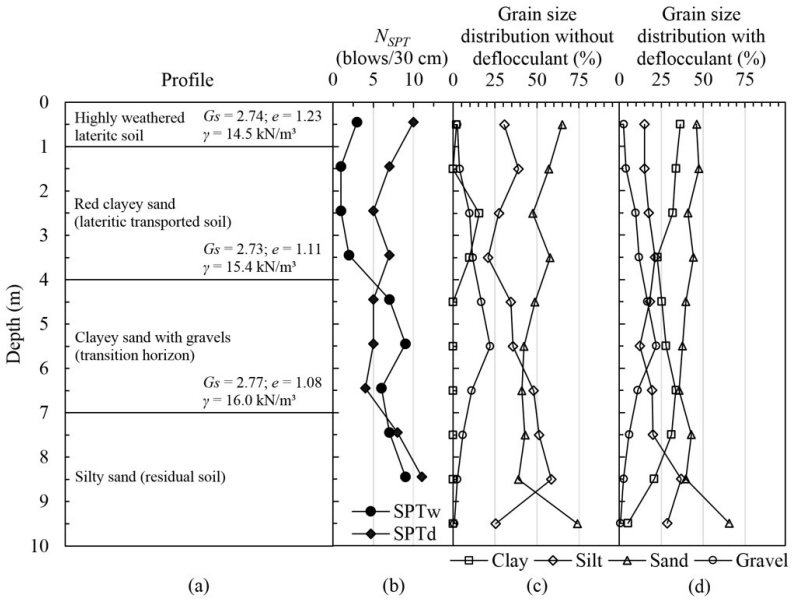

Figure 1. Characteristics of the soil profile of the experimental field: (a) stratigraphy and index properties; (b) SPT test results; (c) grain size distribution without deflocculant and (d) with deflocculant. Modified after Nascimento (2019) and Machado et al. (2020).

deflocculant (sodium hexametaphosphate, for the fraction passing through a no. 10 sieve or 75 μm) showed that in some layers the clay particles are 100% aggregated.

Standard penetration tests (SPT) were performed in the experimental field in the wet season (Machado et al., 2018) and also in the dry season (Rezende & Rocha, 2020) of the local rainfall regime (Figure 1b). In the lateritic soil layer, an increase in N_{SPT} was recorded from 1–3 blows in the wet season (SPT_w) to 5–10 blows in the dry season (SPT_d), evidencing the influence of matric suction on soil strength. The water table was not identified during all the tests, carried out until 10 m depth.

In the experimental field, Ménard-type (or pre-bored) pressuremeter tests (PMT), were also performed at depths of 0.5, 1.5, 2.5, 3.5, 4.5, and 5.5 (Bernardes et al., 2022). Figure 2 shows the pressuremeter curves of two PMT soundings with 6 tests performed on each, both carried out in the dry season. The corrected measured pressure is plotted on the vertical axis and the relative increase in cavity radius (ε_r) on the horizontal axis. Due to inconsistent results, PMT-2 performed at the 4.5 m depth (Figure 2b) was excluded from the graph. Data from these tests were used to estimate some parameters of the constitutive model, as will be discussed in Section 3.2.

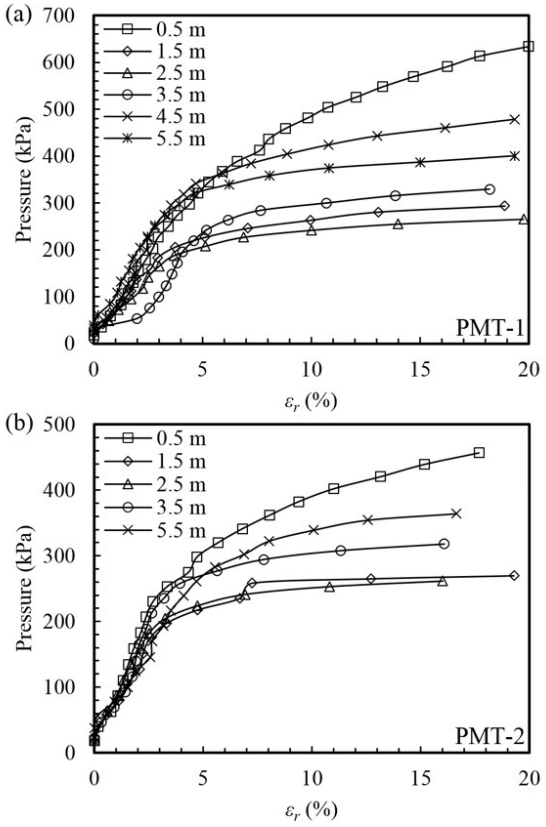

Figure 2. Pressuremeter curves of (a) PMT-1 and (b) PMT-2. Modified after Bernardes et al. (2022).

2.2 Test piles

The static load tests analyzed in this paper were conducted on three DCIS piles (C4, C6, and C8). As illustrated in Figure 3a, these piles are installed by driving or, as in the present case, by jacking a closed-ended steel tube into the ground. The tube is extracted after reaching the required penetration depth. Then the rebar cage is lowered, and the cavity is filled with concrete. Both the installation and the load tests were performed during the dry season of the local rainfall regime.

The piles C4, C6, and C8 are respectively 114.3 mm, 165.1 mm, and 219.1 mm in diameter, and all three piles are 3.5 m in length. A 0.5 m deep shallow excavation was made at the locations of the piles, due to a large amount of organic soil in this layer. Thus, the piles were installed between 0.5–4.0 m deep concerning the natural profile

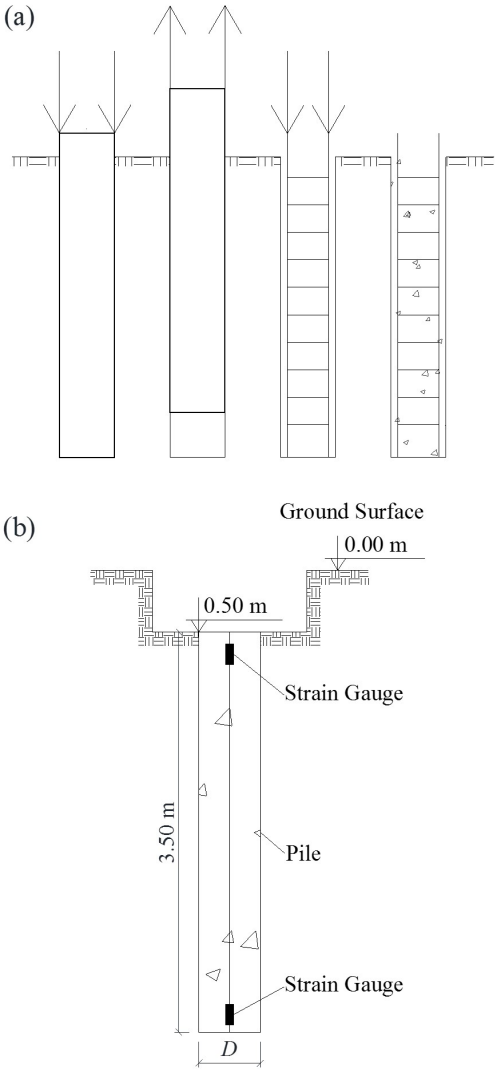

Figure 3. Schematic sketch of: (a) DCIS piles constructive sequence; (b) DCIS piles installed in the experimental field.

(Figure 3b). The piles C6 and C8 were instrumented with strain gauges positioned 100 mm from the top and bottom of the pile (Figure 3b).

As can be seen in Figure 4, the piles and in-situ tests were located close to each other. Therefore, it was considered that the stratigraphy and soil parameters do not vary significantly in the location of each pile and that the average index values obtained from the same type of test (e.g., PMT) are representative of the entire area.

3. Numerical modeling

3.1 Description of the model

The numerical analyses conducted in this paper were carried out in Plaxis 2D® finite element software, with axisymmetric geometry. The horizontal and vertical boundaries limits of the domain were set as 3 and 4 times the pile length, respectively. The model domain is discretized by 15-node triangular elements. A denser mesh was used within the pile structure and in a zone of 6*D* horizontally from the pile shaft and 3*D* below the pile tip, being *D* the pile diameter (Figure 5). Both the domain boundaries and the mesh density were determined by sensitivity analyses.

The groundwater table was not considered, since it was not identified in in-situ tests up to 10 m, so the numerical analyses were conducted under drained conditions. The geostatic stresses are determined using the K_0-procedure, in which the vertical stresses are generated in equilibrium with the self-weight of the soil and the horizontal stresses are calculated from the specified value of the coefficient of earth pressure at rest, K_0.

For proper modeling of pile-soil interaction, interface elements were placed between the pile and soil. In Plaxis 2D®, the interface behavior is described by an elastoplastic model with the Mohr-Coulomb failure criterion. The interface shear strength is related to the soil shear strength by the strength reduction factor, R_{inter}, which can reduce the interface cohesion and friction angle ($R_{inter} < 1$) or keep it equal to that of the surrounding soil ($R_{inter} = 1$).

3.2 Estimation of the constitutive model parameters

Soil behavior is described by the elastoplastic Hardening Soil (HS) constitutive model (Schanz et al., 1999). Among the basic features of the HS model that motivated its adoption are the stress dependency of stiffness and the use of different stiffness modulus for virgin loading and unloading/reloading conditions. By its characteristics, the HS model has proven superior to an elastic perfectly-plastic model in modeling piles in finite element analysis (Broere & van Tol, 2006; Wehnert & Vermeer, 2004).

Conventionally, the parameters of the HS model are calibrated via triaxial and oedometer tests. In practice, the feasibility of these tests is often limited due to difficulties related to soil sampling or the complexity and cost of testing, especially for geotechnical problems involving the characterization of thick soil layers. Thus, laboratory tests are often replaced by field tests, such as PMT and SPT, whose results can be used to estimate the model parameters

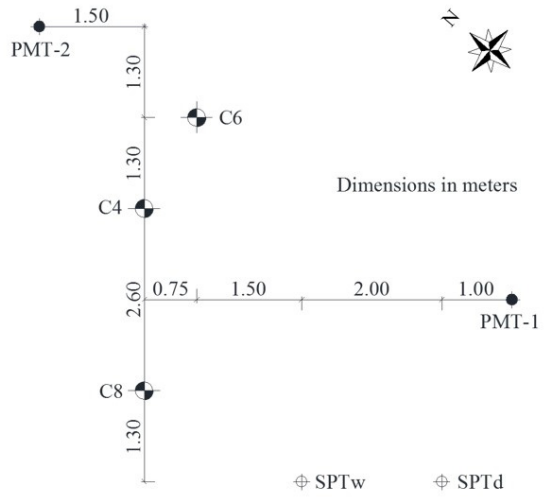

Figure 4. The relative position of the DCIS piles and in-situ tests located in the experimental field (dimensions in meters).

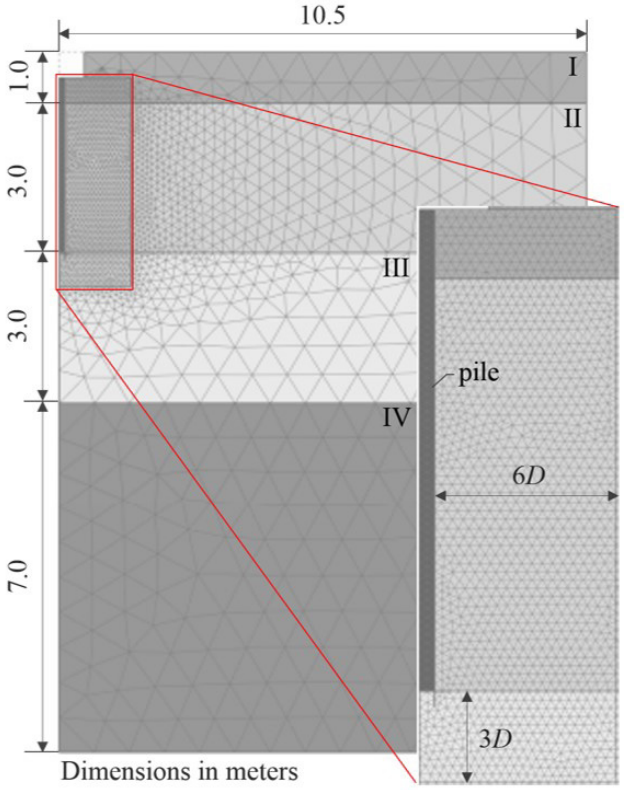

Figure 5. Finite element mesh discretization (dimensions in meters).

through numerical techniques or empirical correlations, but the latter must be used with care. In the present work, the input parameters of the HS model were estimated using different methods: interpretation of field tests using both numerical techniques and empirical correlations; default values suggested by Plaxis 2D®; reference values found in the literature.

The HS model has eleven input parameters, which can be divided between strength, stiffness, and advanced parameters. The first group includes the cohesion (c), the friction angle (ϕ), and the angle of dilatancy (ψ). The stiffness parameters are the reference stiffness modulus related to primary deviatoric loading (E_{50}^{ref}), primary compression (E_{oed}^{ref}) and unloading/reloading (E_{ur}^{ref}), and the stiffness power law exponent, m, which defines the stiffness dependence on the stress level.

The advanced parameters of the HS model are the reference confining pressure (p^{REF}), the Poisson's ratio for unloading/reloading (υ_{ur}), the failure ratio (R_f), and the coefficient of earth pressure at rest for normal consolidation (K_0^{NC}), for which default values suggested by Plaxis 2D® were used.

The angle of dilatancy is set equal to zero for all soil layers. This assumption agrees with what has been observed for tropical soil profiles from the Center-West region of Brazil such as the soil profile of the experimental field (Bernardes et al., 2022; Rebolledo et al., 2019).

The parameters c, ϕ, and E_{50}^{ref} of the first three layers were determined through the methodology for numerical simulation of pressuremeter tests proposed by Goulart (2021). The method allows estimating Young's modulus, apparent cohesion, and friction angle of the soil through a curve-fitting approach. As an approximation, the parameter E_{50}^{ref} was set equal to the stiffness modulus obtained through this technique. It should be noted that despite considering drained conditions in the numerical analyses, apparent cohesion was used instead of effective cohesion to indirectly incorporate the effect of matric suction.

As mentioned in Section 2.1, the pressuremeter tests were performed up to 5.5 m depth, so no data were available for estimating the parameters c, ϕ, and E_{50}^{ref} of the fourth layer (7–14 m depth) using the methodology of Goulart (2021). Due to the length of the piles (3.5 m), the variation of parameters in this layer has little influence on the results. Therefore, it was decided to estimate the modulus E_{50}^{ref} of this layer through an empirical correlation with the N_{SPT} value of SPT_d (Figure 1a). As an approximation, this parameter was considered equal to the modulus obtained by the relation $E = \alpha\beta N_{SPT}$, proposed by Teixeira & Godoy (1998), where α and β are soil-dependent coefficients, which for silty sands are equal to 0.7 and 3.0, respectively. The other parameters were considered equal to those of the third layer (4–7 m depth), which are discussed below.

The other stiffness parameters (E_{oed}^{ref}, E_{ur}^{ref}, and m) were estimated based on simplifications considered valid for medium to dense silty sands (Schmüdderich et al., 2020) and tropical sandy soils of the Center-West region of Brazil (Bernardes et al., 2022; Rebolledo et al., 2019). For all soil layers, the modulus E_{oed}^{ref} and E_{ur}^{ref} were obtained by the relations $E_{oed}^{ref}/E_{50}^{ref} = 1$ and $E_{ur}^{ref}/E_{50}^{ref} = 3$, respectively, and the exponent m is set equal to 0.5.

In addition to the HS model parameters, the unit weight of moist soil (γ), the coefficient of earth pressure at rest (K_0), and the overconsolidation ratio (OCR) are also input parameters. The parameters γ and K_0 were determined by Machado (2020) to a depth of 5.5 m. The former through laboratory tests and the latter through PMT results. The OCR was estimated using Equation 1 (Mayne & Kulhawy, 1982; Schmidt, 1966). Again, the parameters of the fourth layer were considered equal to those of the third layer. A summary of the model parameters for each layer is provided in Table 1.

$$K_0 = K_0^{NC} OCR^{\sin\phi} \quad (1)$$

The behavior of the concrete piles is assumed linear elastic, with a unit weight of 24 kN/m³, a Poisson's ratio of 0.2, and Young's modulus equal to 21 GPa.

3.3 Approaches for numerical simulation of full-displacement piles

The numerical approaches proposed in this paper for simulating the installation and axial loading of DCIS piles are the result of modifications made to pre-existing methods. As will be discussed in the next sections, the original approaches were initially calibrated for

Table 1. Parameters of the constitutive model.

Layer	Depth	γ	c	ϕ	E_{50}^{ref}	E_{oed}^{ref}	E_{ur}^{ref}	K_0^{NC}	K_0	OCR
	(m)	(kN/m³)	(kPa)	(°)	(kPa)	(kPa)	(kPa)	-	-	-
1	0 - 1	14.5	58	30	17053	17053	51158	0.51	2.34	22.2
2	1 - 4	15.4	24	30	7537	7537	22610	0.50	0.68	1.9
3	4 - 7	16.0	50	31	11755	11755	35266	0.49	0.50	1.0
4	7 - 14	16.0	50	31	19950	19950	59850	0.49	0.50	1.0

Constant model parameters: $\psi = 0; \upsilon_{ur} = 0.2; R_f = 0.9; p^{ref} = 100\ kPa$; K_0^{NC}=1-sen(ϕ). Columns 3 and 10: data from (Machado, 2020). Columns 4 to 6: data from (Goulart, 2021).

the analysis of screw displacement piles (i.e., SDP or "Omega" piles). Thus, these methods have been modified to better incorporate the installation effects of DCIS piles. The calculation steps of each method employed in this work (original and modified) are shown in Figure 6. The original methods are discussed in Sections 3.3.1 and 3.3.2, while the proposed approaches are presented in detail in Sections 3.3.3 and 3.3.4.

3.3.1 Cavity Expansion (CE) method

This method was initially proposed by Krasinski (2014) and later employed by Schmüdderich et al. (2020) for the finite element simulation of SDP. Its basic principle consists in simulating the radial displacements induced in the soil by the displacement auger through the expansion process of a cylindrical cavity. The calculation steps are illustrated in Figure 6a.

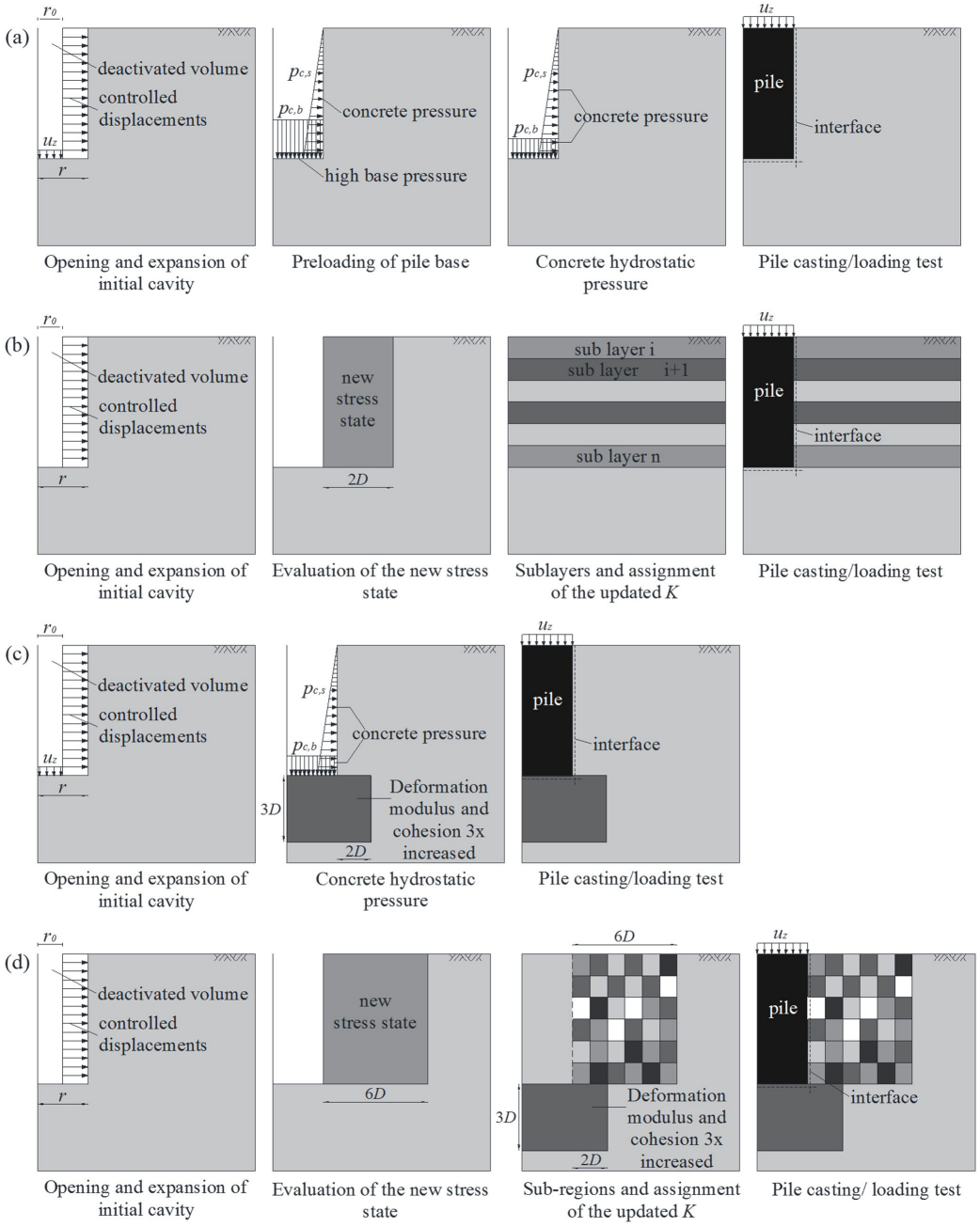

Figure 6. Calculation steps of the original Cavity Expansion (a) and Cavity Expansion with Sub-Layering (b) methods (modified after Schmüdderich et al., 2020) and of the proposed Cavity Expansion with Base iImprovement (c) and Cavity Expansion with Sub-Regions (d) methods.

After the generation of geostatic stresses by the K_0-procedure, an initial cavity is created by deactivating a soil volume with a radius r_0, equal to $r/2$ (r = pile radius). The adoption of an adequate value of r_0 is important in this step. The smaller the r_0, the greater the expanded soil volume, which approximates the actual pile installation process, in which the displaced soil volume is equal to the pile volume (situation equivalent to $r_0 = 0$). However, very small r_0 values can lead to numerical problems due to mesh distortions. Krasinski (2014) determines the value of r_0 through trials. In the present work, the r_0 value was reevaluated for the case study, and the most appropriate value remained equal to $r/2$.

Simultaneously with the creation of the initial cavity, a displacement boundary condition of $\Delta = r - r_0$ is applied to the cavity wall, resulting in a final cavity of radius r. Moreover, to avoid stress concentrations and mesh distortions around the top and bottom of the pile, Krasinski (2014) gradually decreases the displacements to zero by forming a triangular distribution of 0.5 m height on both ends of the cavity. However, it was found that this procedure impairs the final geometry of the head and base of the pile, as well as the continuity of the interface elements in the pile shaft. Figure 7 shows a zoomed view of the pile base region illustrating this effect. Therefore, in the present work, a uniform distribution was applied, and to suppress any unwanted mesh distortions at the bottom of the cavity, very small vertical displacements (of the order of 0.1 mm) were also applied at the bottom of the initial cavity in the expansion phase. These vertical displacements were determined through trials, aiming to obtain a value that was sufficient to prevent mesh deformations and that did not interfere with the results.

The concreting phase is simulated next by applying a horizontal pressure p_{cs} to the cavity wall and a vertical pressure p_{cb} to the cavity base. The magnitude of p_{cs} was set equal to the hydrostatic pressure of the fresh concrete. Since it was not possible to incorporate the stresses induced by the penetration of the SDP displacement auger around the bottom of the cavity in the expansion phase, a value of p_{cb} considerably higher than the hydrostatic concrete pressure was first applied. Then, in the next step, the base pressure was reduced to the hydrostatic pressure of the concrete. In this way, a preconsolidation effect under the pile tip is obtained.

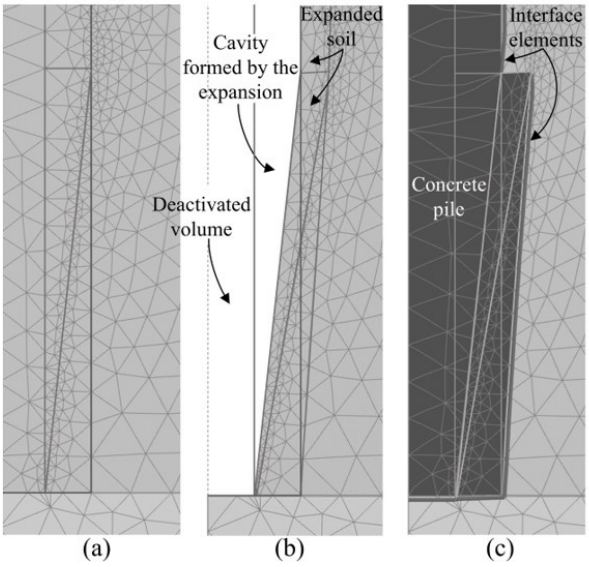

Figure 7. Final geometry of the pile base when the displacement distribution is triangular at the cavity ends: (a) initial phase; (b) after expansion; (c) after pile casting.

Krasinski (2014) calibrates the highest p_{cb} value through trials to obtain the field-measured pile base resistance. In this work, it was not possible to reach a p_{cb} value that was sufficient to obtain a base resistance consistent with the experimental results without generating excessive deformation of the soil below the cavity bottom. Thus, the value adopted by Krasinski (2014) of p_{cb} = 1800 kN/m² was used in the analyses.

To model the pile, concrete properties are assigned to the soil volume that had initially been deactivated. Simultaneously, the interface elements are activated. Finally, a static load test is simulated by applying prescribed displacements at the top of the pile.

Furthermore, Krasinski (2014) assumes a zone around the pile shaft with reduced stiffness parameters. This assumption was not made in this work since, as will be discussed later, the pile load capacity obtained without reductions in the interface strength (R_{inter} = 1) was already lower than that verified experimentally. It should be noted that all calculation steps use the updated mesh option available in Plaxis 2D®.

3.3.2 Cavity Expansion with Sub-Layering (CE-SL) method

Introduced by Schmüdderich et al. (2020) for finite element analysis of SDP, the original approach (Figure 6b) simulates the pile installation process and the subsequent load test in two separate numerical models so that installation effects are considered indirectly in a model that has not undergone finite element mesh deformation. In the first model, the radial displacements induced in the ground by the displacement auger are simulated as the expansion of a cylindrical cavity, as in the CE approach. The post-expansion radial stresses within a zone of $2D$ (D = pile diameter) around the pile shaft are used to calculate an updated coefficient of lateral earth pressure profile, K.

The value of r_0 used by Schmüdderich et al. (2020) is calculated based on the geometry of the SDP displacement auger, so the same logic does not apply to DCIS piles. Therefore, a value of r_0 equal to $r/2$ was adopted for this method as well. Furthermore, the original approach also gradually decreases the horizontal displacements applied in the expansion phase near the top and bottom of the cavity, which is not adopted in the present work for the reasons already exposed in the CE approach.

In a second model, the soil adjacent to the pile shaft is divided into 1 m thick sub-layers and for each is assigned an

average *K* value obtained from the previous model. Then, the pile is installed wished-in-place by assigning the concrete properties to the soil volume representing it, and the interface elements are activated. As will be discussed later, in this approach, it was necessary to reduce the interface strength by 40% (R_{inter} = 0.60). Finally, a load test was simulated as discussed in the previous section.

3.3.3 Cavity Expansion with Base Improvement (CE-BI) method

The first approach proposed in this paper is the result of modifications made to the CE method. In the new approach (Figure 6c), the cavity expansion phase remains the same as in the original approach. After expansion, the phase in which hydrostatic concrete pressures are applied to the base and the cavity wall follows. The phase of pre-consolidation of the base is suppressed. Instead, to obtain the densification effect in this region, a zone is created below the pile tip in which the stiffness modulus (E_{50}^{ref}, E_{oed}^{ref}, and E_{ur}^{ref}) and soil cohesion are increased 3 times. Experimental results from model piles indicate that the main strains occurring below the pile tip are within a zone extending vertically from 2 to 4*D* and radially from 1 to 3*D* from the pile axis (Liu et al., 2020; White & Bolton, 2004). Thus, a zone extending 3*D* below the pile tip and 2.5*D* in the side direction from the pile axis was adopted. Furthermore, this zone comprises the main vertical stresses developed due to pile loading. As shown in Figure 8, the isobar corresponding to 5% of the mean vertical pressure acting at the pile tip (σ_b) is within this zone.

The magnitude of the parameters increase was determined by trial and error to obtain base resistances consistent with experimentally measured values of pile C6. The shearing that occurs in the cavity wall due to the jacking and subsequent extraction of the closed-ended steel tube is not considered in the analyses. The last two phases (pile casting and load test) remain unchanged.

The interface shear strength was considered equal to that of the surrounding soil (R_{inter} = 1). Despite the absence of laboratory tests to determine the interface friction angle (δ), the evidence found in the literature indicates that the assumption made is close to reality. Experimental studies suggest that the interface friction angle between sandy soils and rough surfaces (such as that of the shaft of cast-in-situ piles) is close to the soil friction angle so that under external loads, shearing tends to occur within the soil mass adjacent to the pile shaft and not at the pile-soil interface (Flynn & McCabe, 2016; Frost et al., 2002; Martinez & Frost, 2017).

Moreover, the phenomenon of friction fatigue on displacement piles depends on several factors, such as soil type, surface roughness, and pile installation technology (Randolph et al., 1994; White & Lehane, 2004). Dynamic installation techniques that induce cyclic shearing at the pile shaft, such as pile driving, cause greater degradation of the shaft friction than a monotonic or jacked installation (White & Lehane, 2004). Materials with smooth surfaces (such as steel) also cause less degradation than those with rough surfaces (Tovar-Valencia et al., 2018). Considering that the installation process of the DCIS piles analyzed in the present work involves the jacking of closed-ended steel tubes, the authors of the current study considered it reasonable to expect less severe friction fatigue in this case.

3.3.4 Cavity Expansion with Sub-Regions (CE-SR) method

The CE-SR method (Figure 6d) is the result of modifications made to the CE-SL method. The first modification was the introduction of a zone below the pile base with improved soil stiffness and strength parameters. The amount of parameter increase and the size of the zone is the same as in the CE-BI approach.

The other modifications are related to the way that changes in radial stresses in the soil adjacent to the pile shaft are considered. The stress reading was expanded to 6*D* horizontally from the pile shaft. The soil adjacent to the pile shaft was divided into 0.5 m thick sub-layers, which was motivated by the shorter length of the piles under analysis (3.5 m) compared to the 9.5 m length of the pile analyzed by Schmüdderich et al. (2020). Furthermore, the region to which the updated *K* profile is assigned was limited radially in 6*D* from the pile shaft, with vertical divisions every 1*D*. Each sub-region thus obtained was assigned an average *K* value calculated according to the radial stresses evaluated in the same region.

The extent of this zone was determined after weighing the zone of influence of radial stresses (σ_r) induced by

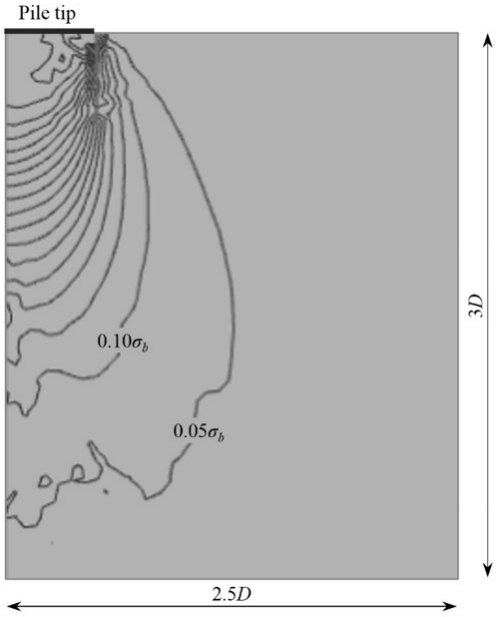

Figure 8. Pressure bulb due to pile loading for pile C8.

the cavity expansion and the applicability of the method. Figure 9 shows curves of the radial stresses of the soil adjacent to the C6 pile shaft before and after the cavity expansion phase for two depth levels (1.5 and 3.5 m). It can be seen that from a radial distance of the order of 6*D*, the increment in radial stresses induced by the expansion is low and tends to constancy for greater distances.

The last two calculation steps (pile casting and load test) remain unchanged. However, in the modified approach, the interface shear strength was not reduced (R_{inter} = 1), for the reasons previously discussed for the CE-BI approach.

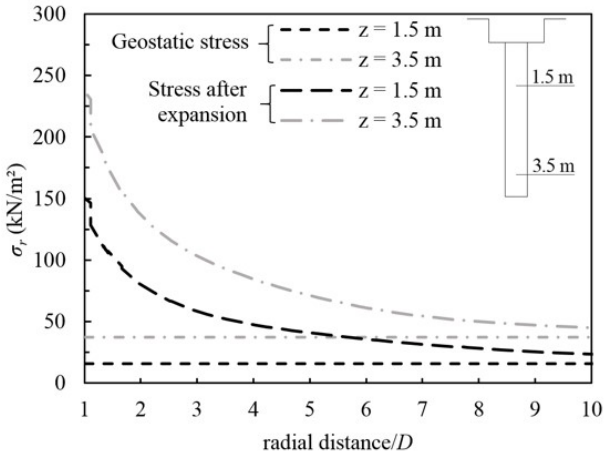

Figure 9. Radial stresses pre and post cavity expansion for pile C6.

4. Analysis and results

4.1 Original CE and CE-SL methods

The load-settlement curves measured in the field and obtained with the numerical approaches are presented in Figure 10. The bearing capacity of piles C4, C6, and C8 obtained with the CE approach was approximately 17% lower than the values verified in the field (Figure 10a). On the other hand, with the CE-SL approach, it was necessary to reduce the interface shear strength to 60% of the mobilized shear strength in the surrounding soil (R_{inter} = 0.60) to obtain failure values close to those measured experimentally (Figure 10b). The load-settlement behavior for settlements < 5 mm was similar with both methods for all piles.

Figure 11 shows the mobilization of the average shear stress at the pile shaft and of the pile base pressure with the evolution of the pile head settlements (w), which were normalized by the pile diameter. Both the results computed with the numerical approaches and those measured in the field are presented. The numerical results for pile C4 are also shown, although no experimental data were available for comparison due to the lack of instrumentation on this pile.

For settlements greater than 0.02*D*, both numerical approaches predict greater shaft friction mobilization than verified in the field. At failure conditions, while the CE method (Figure 11a) predicts a reasonable shaft friction mobilization relative to field-measured values, the CE-SL method (Figure 11b) considerably overestimates these values. Concerning the pile base pressure, both methods resulted in

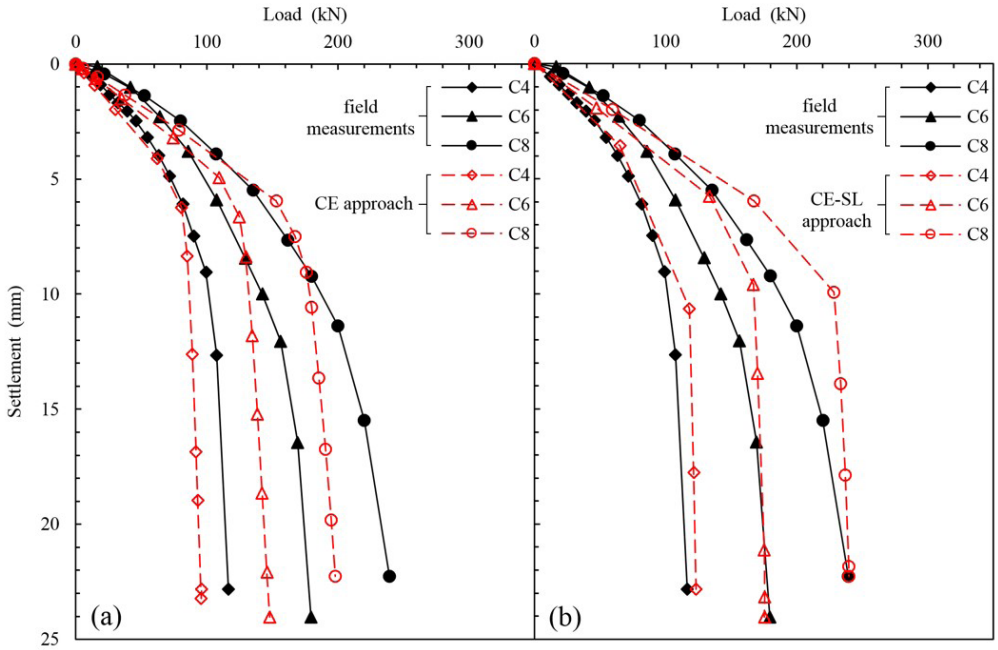

Figure 10. Comparison of load-settlement curves for (a) CE approach and (b) CE-SL approach.

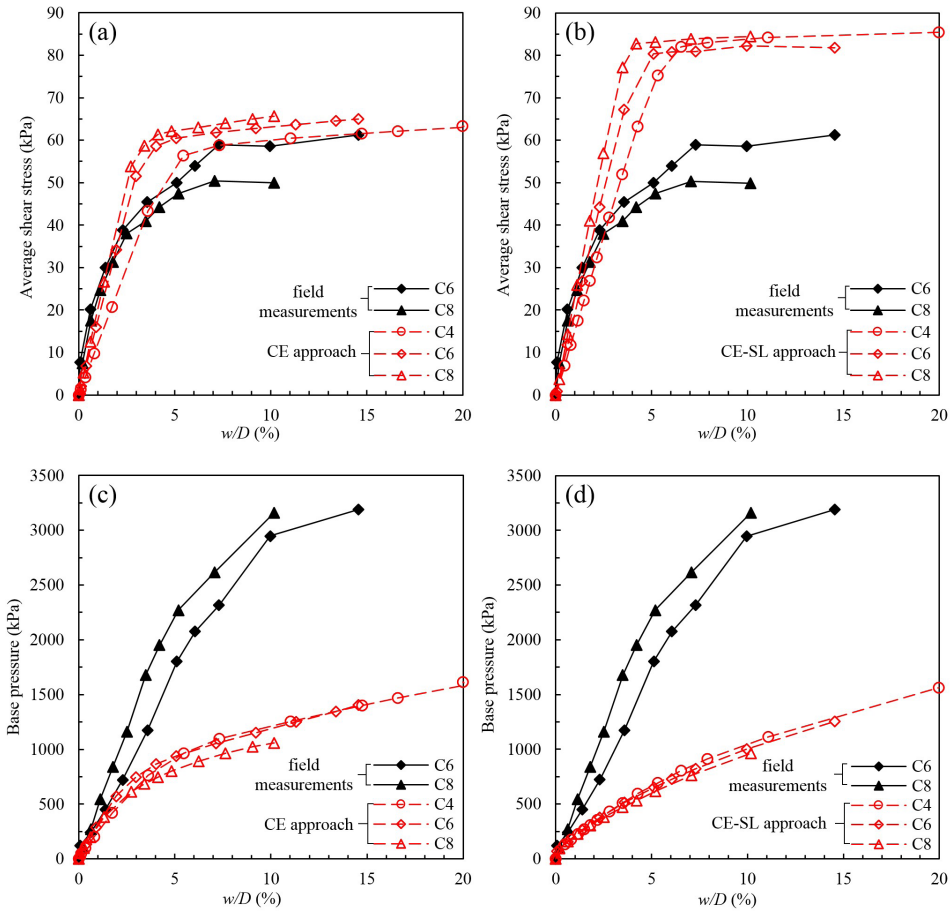

Figure 11. Average shear stress at the pile shaft for (a) CE approach and (b) CE-SL approach and pile base pressure for (c) CE approach and (d) CE-SL approach.

similar behavior, underestimating the base resistance of the piles. This underestimation was the main reason for the error in the estimation of the bearing capacity of the piles with the CE method. Furthermore, the base pressure mobilization computed from the numerical models was quite similar among the piles, regardless of pile diameter, with a slightly lower mobilization for pile C8.

These results are attributed to the fact that both approaches were originally developed for the analysis of SDP, whose installation technology differs from the DCIS piles. In the case of driven or jacked piles, the stress state of the soil below the pile base is greatly influenced by the installation, while in the case of SDP the soil adjacent to the pile shaft is more affected (Krasinski, 2014). Moreover, Flynn & McCabe (2016) reported that the shaft friction mobilization mechanisms of DCIS piles installed in sandy soils are closer to those of bored piles, due to the rough shaft surface resulting from in-situ concreting and the absence of residual stresses related to the driving process, since in the case of DCIS piles, the installation tube is extracted before concreting.

4.2 Proposed CE-BI and CE-SR methods

Figure 12 shows the load-settlement curves measured in the field and obtained with the proposed numerical approaches. Despite the differences between the methods, both resulted in quite similar behavior. In terms of bearing capacity, the numerical results were very reliable when compared to those measured experimentally, with errors ranging from 1% to 3% for both approaches. It can be seen from the load-settlement curves for piles C4 to C8, that for settlements between about 2% and 6% of the pile diameter, both numerical models result in a stiffer stress-strain behavior than the one observed in the field, especially the CE-SR method.

Modifications made to the CE-SL approach in the way of incorporating the installation effects around the pile shaft improved the prediction of shear stress mobilization (Figure 13b), although both numerical approaches still slightly overestimate the shaft resistance of the piles. In addition, the numerical models predict a shear stress mobilization proportional to the pile diameter, with a trend more evident for the CE-BI method (Figure 13a).

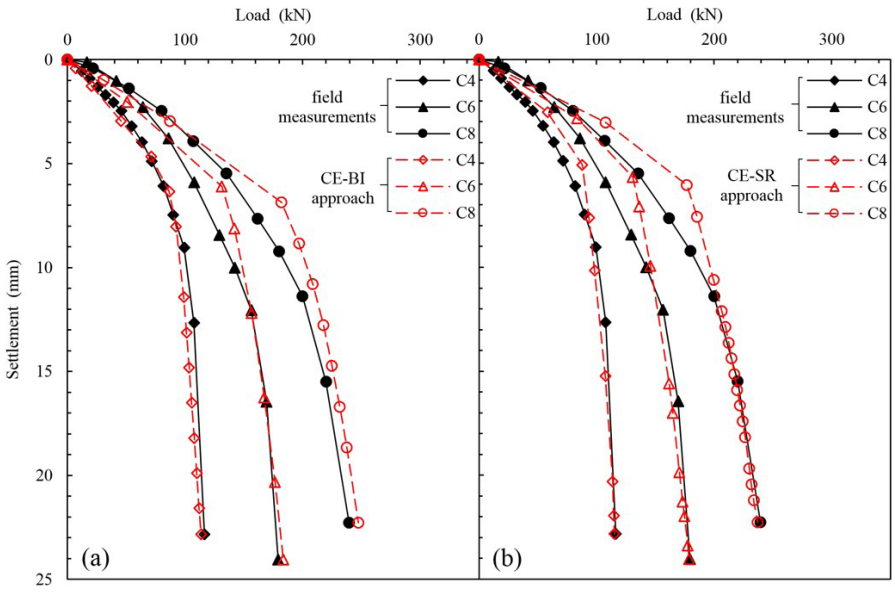

Figure 12. Comparison of load-settlement curves for (a) CE-BI approach and (b) CE-SR approach.

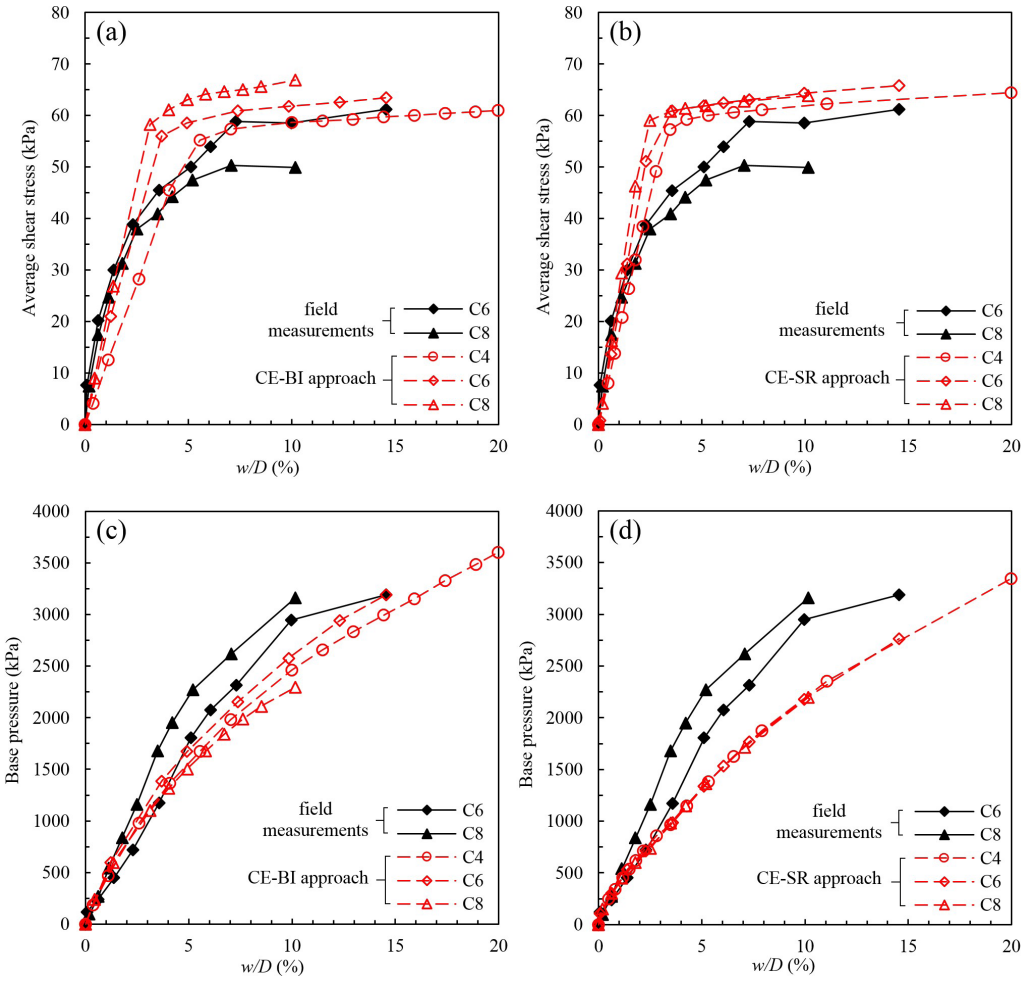

Figure 13. Average shear stress at the pile shaft for (a) CE-BI approach and (b) CE-SR approach and pile base pressure for (c) CE-BI approach and (d) CE-SR approach.

The increase of the stiffness parameters and the soil cohesion below the piles tips allowed a better mobilization of the base pressure, with the CE-BI method predicting slightly higher values. At failure conditions, the base resistance obtained with the CE-BI method (Figure 13c) was quite accurate for pile C6, while in the case of pile C8 there was an underestimation of 27%. With the CE-SR method (Figure 13d), the errors in estimating the ultimate base resistance of piles C6 and C8 were 13% and 30%, respectively. These results highlight the importance of considering soil densification below the pile base in numerical modeling of DCIS piles.

5. Conclusions

This paper proposed two numerical approaches for finite element analysis of DCIS piles that allow incorporating the installation effects in an idealized manner. The approaches, named CE-BI and CE-SR methods, are the result of improvements made to preexisting methods. The modified approaches introduce a densified zone under the pile tip and improve the way of incorporating the installation-induced changes in radial stresses of the surrounding soil. The results obtained allow the following conclusions:

- Both proposed numerical approaches were able to satisfactorily reproduce axial load tests conducted on DCIS piles, being sensitive to pile diameter variation. The numerical bearing capacity predictions showed an average error of 2% compared to the measured values. In the failure conditions, the models accurately obtained the pile shaft and base resistances. The average error between measured and numerical values was 18% for both shaft and base resistances. In the case of base resistance, this is due to an overestimation, while in the case of shaft resistance it is due to an underestimation of the values. In terms of relative pile-soil stiffness, there was a slightly overestimated response for intermediate loading stages.
- Despite the methodological differences between the approaches, both result in a behavior that is quite similar to each other. In terms of applicability, the CE-BI method has the advantage of being modeled in a single numerical model. However, due to distortions of the finite element mesh in the cavity expansion and pile casting phases, the method may present some numerical instabilities that do not occur in the CE-SR method, since the latter separates the cited stages into two different models. Under these circumstances, the CE-SR method is superior to the CE-BI method.
- To apply the methods for predicting the behavior of displacement piles under axial compression loads, the limiting factor is the need for data that can be used to calibrate the characteristics of the pile-soil interface and to determine the magnitude of the increase in soil strength and stiffness parameters in the improved zone below the pile base. An instrumented load test, such as those used in this paper, is an adequate tool for this purpose.

Acknowledgements

The authors thank the Brazilian sponsorship organizations CAPES (Coordination for the Improvement of Higher Education) and CNPq (National Council for Scientific and Technological Development) for the financial support and Eletrobras FURNAS for the technical cooperation with UFG.

Declaration of interest

The authors have no conflicts of interest to declare.

Authors' contributions

Bismarck Chaussê Oliveira: conceptualization, data curation, formal analysis, methodology, validation, visualization, writing – original draft. Maurício Martines Sales: conceptualization, methodology, supervision, validation, riting – review & editing. Renato Resende Angelim: investigation, writing – review & editing. Luiz Carlos Galvani Junior: investigation, writing – review and editing.

Data availability

All data produced or examined in the course of the current study are included in this article.

List of symbols

c	Soil cohesion
D	Pile diameter
e	Void ratio of soil
E	Young's modulus
E_{50}^{ref}	Reference stiffness modulus for primary deviatoric loading
E_{oed}^{ref}	Reference stiffness modulus for primary compression
E_{ur}^{ref}	Reference stiffness modulus for unloading/reloading
G_s	Specific gravity of soil
K	Coefficient of lateral earth pressure
K_0	Coefficient of earth pressure at rest
K_0^{NC}	Coefficient of earth pressure at rest for normal consolidation
m	Stiffness power law exponent
N_{SPT}	SPT N-value
OCR	Overconsolidation ratio
$p_{c,s}$	Horizontal pressure at cavity wall
$p_{c,b}$	Vertical pressure at cavity bottom
p^{REF}	Reference confining pressure
r	Pile radius
r_0	Initial cavity radius

R_f	Failure ratio
R_{inter}	Interface strength reduction factor
w	Pile head settlement
α	Teixeira & Godoy (1998) first soil-dependent coefficient
β	Teixeira & Godoy (1998) second soil-dependent coefficient
γ	Unit weight of moist soil
δ	Interface friction angle
ε_r	Relative increase in cavity radius measured in the pressuremeter tests
σ_b	Mean vertical pressure at the pile base
σ_r	Radial stress
υ_{ur}	Poisson's ratio for unloading/reloading
ϕ	Friction angle of soil
ψ	Angle of dilatancy of soil

References

Bernardes, H.C., Sales, M.M., Machado, R.R., Cruz Junior, A.J., Cunha, R.P., Angelim, R.R., & Rebolledo, J.F.R. (2022). Coupling hardening soil model and Ménard pressuremeter tests to predict pile behavior. *European Journal of Environmental and Civil Engineering*, 26(11), 5221-5240. http://dx.doi.org/10.1080/19648189.2021.1886180.

Brinkgreve, R. B. J., Kumarswamy, S., Swolfs, W. M., Fonseca, F., Monoj, N. R., Zampich, L., & Zalamea, N. (2021). *Plaxis connect edition: general information manual*. Plaxis bv.

Broere, W., & van Tol, A.F. (2006). Modelling the bearing capacity of displacement piles in sand. *Proceedings of the Institution of Civil Engineers - Geotechnical Engineering*, 159(3), 195-206. http://dx.doi.org/10.1680/geng.2006.159.3.195.

Camapum de Carvalho, J., & Gitirana Junior, G.F.N. (2021). Unsaturated soils in the context of tropical soils. *Soils and Rocks*, 44(3), 1-25. http://dx.doi.org/10.28927/SR.2021.068121.

Engin, H.K. (2013). *Modelling pile installation effects - a numerical approach* [Doctoral thesis]. Delft University of Technology. https://doi.org/10.4233/uuid:3e8cc9e2-b70c-403a-b800-f68d65e6ea85.

Engin, H.K., Brinkgreve, R.B.J., & van Tol, A.F. (2015). Simplified numerical modelling of pile penetration – the press-replace technique. *International Journal for Numerical and Analytical Methods in Geomechanics*, 39(15), 1713-1734. http://dx.doi.org/10.1002/nag.2376.

Flynn, K.N., & McCabe, B.A. (2016). Shaft resistance of driven cast-in-situ piles in sand. *Canadian Geotechnical Journal*, 53(1), 49-59. http://dx.doi.org/10.1139/cgj-2015-0032.

Freitas, J.B., Rezende, L.R., & Gitirana Junior, G.F.N. (2020). Prediction of the resilient modulus of two tropical subgrade soils considering unsaturated conditions. *Engineering Geology*, 270, 105580. http://dx.doi.org/10.1016/j.enggeo.2020.105580.

Frost, J.D., DeJong, J.T., & Recalde, M. (2002). Shear failure behavior of granular-continuum interfaces. *Engineering Fracture Mechanics*, 69(17), 2029-2048. http://dx.doi.org/10.1016/S0013-7944(02)00075-9.

Goulart, R.L. (2021). *Análise numérica de ensaios pressiométricos do campo experimental da EECA* [Unpublished master's dissertation]. Federal University of Goiás (in Portuguese).

Heins, E., & Grabe, J. (2017). Class-A-prediction of lateral pile deformation with respect to vibratory and impact pile driving. *Computers and Geotechnics*, 86, 108-119. http://dx.doi.org/10.1016/j.compgeo.2017.01.007.

Krasinski, A. (2014). Numerical simulation of screw displacement pile interaction with non-cohesive soil. *Archives of Civil and Mechanical Engineering*, 14(1), 122-133. http://dx.doi.org/10.1016/j.acme.2013.05.010.

Li, Y., Liu, C., & Song, J. (2021). The pile end mechanism of jacked pile in layered soils. *Indian Geotechnical Journal*, 51, 1087-1098. http://dx.doi.org/10.1007/s40098-021-00510-1.

Liu, C., Tang, X., Wei, H., Wang, P., & Zhao, H. (2020). Model tests of jacked-pile penetration into sand using transparent soil and incremental particle image velocimetry. *KSCE Journal of Civil Engineering*, 24(4), 1128-1145. http://dx.doi.org/10.1007/s12205-020-1643-4.

Lobo-Guerrero, S., & Vallejo, L.E. (2005). DEM analysis of crushing around driven piles in granular materials. *Geotechnique*, 55(8), 617-623. http://dx.doi.org/10.1680/geot.2005.55.8.617.

Lorenzo, R., Cunha, R.P., Cordão Neto, M.P., & Nairn, J.A. (2018). Numerical simulation of installation of jacked piles in sand using material point method. *Canadian Geotechnical Journal*, 55(1), 131-146. http://dx.doi.org/10.1139/cgj-2016-0455.

Machado, R.R. (2020). *Ensaios pressiométricos para estimativa de parâmetros de resistência e deformabilidade do solo do campo experimental da EECA/UFG* [Unpublished master's dissertation]. Federal University of Goiás (in Portuguese).

Machado, R.R., do Nascimento, B.B., Rodrigues, J.L. da M., Angelim, R.R., Sales, M.M., Lima Junior, J.C., Merighi, V.A., & Fonseca, A.L.E. (2018). Medição de energia em ensaio SPT realizado no campo experimental da EECA/UFG. In *19° Congresso Brasileiro de Mecânica dos Solos e Engenharia Geotécnica* (Vol. 3). Salvador: ABMS, CBMR, ISRM & SPG. (in Portuguese)

Machado, R.R., Galvani Junior, L.C., Angelim, R.R., & Sales, M.M. (2020). Utilização de ensaios pressiométricos Ménard para avaliação de um perfil de solo tropical. *Tecnia – Revista de Educação, Ciência e Tecnologia do IFG*, 5(2), 219-243. (in Portuguese)

Martinez, A., & Frost, J.D. (2017). The influence of surface roughness form on the strength of sand-structure interfaces.

Géotechnique Letters, 7(1), 104-111. http://dx.doi.org/10.1680/jgele.16.00169.

Mayne, P.W., & Kulhawy, F.H. (1982). K_0-OCR relationships in soil. *Journal of the Geotechnical Engineering Division*, 108(6), 851-872. http://dx.doi.org/10.1061/AJGEB6.0001306.

Nascimento, B.B. (2019). *Provas de carga estáticas em estacas metálicas tubulares de ponta aberta em um solo tropical* [Unpublished master's dissertation]. Federal University of Goiás (in Portuguese).

Nogami, J.S., & Villibor, D.F. (1995). *Pavimentação de baixo custo com solos lateríticos*. Vilibor. (in Portuguese).

Phuong, N.T.V., van Tol, A.F., Elkadi, A.S.K., & Rohe, A. (2016). Numerical investigation of pile installation effects in sand using material point method. *Computers and Geotechnics*, 73, 58-71. http://dx.doi.org/10.1016/j.compgeo.2015.11.012.

Pucker, T., & Grabe, J. (2012). Numerical simulation of the installation process of full displacement piles. *Computers and Geotechnics*, 45, 93-106. http://dx.doi.org/10.1016/j.compgeo.2012.05.006.

Qiu, G., Henke, S., & Grabe, J. (2011). Application of a Coupled Eulerian-Lagrangian approach on geomechanical problems involving large deformations. *Computers and Geotechnics*, 38(1), 30-39. http://dx.doi.org/10.1016/j.compgeo.2010.09.002.

Randolph, M.F., Dolwin, J., & Beck, R. (1994). Design of driven piles in sand. *Geotechnique*, 44(3), 427-448. http://dx.doi.org/10.1680/geot.1994.44.3.427.

Rebolledo, J.F.R., León, R.F.P., & Camapum de Carvalho, J. (2019). Obtaining the mechanical parameters for the Hardening Soil model of tropical soils in the city of Brasília. *Soils and Rocks*, 42(1), 61-74. http://dx.doi.org/10.28927/sr.421061.

Rezania, M., Nezhad, M.M., Zanganeh, H., Castro, J., & Sivasithamparam, N. (2017). Modeling pile setup in natural clay deposit considering soil anisotropy, structure, and creep effects: case study. *International Journal of Geomechanics*, 17(3), 04016075. http://dx.doi.org/10.1061/(asce)gm.1943-5622.0000774.

Rezende, B.L.M., & Rocha, L.B. (2020). *Influência da energia nos resultados do ensaio SPT* [Unpublished undergraduate final project]. Federal University of Goiás. (in Portuguese).

Rooz, A.F.H., & Hamidi, A. (2019). A numerical model for continuous impact pile driving using ALE adaptive mesh method. *Soil Dynamics and Earthquake Engineering*, 118, 134-143. http://dx.doi.org/10.1016/j.soildyn.2018.12.014.

Said, I., De Gennaro, V., & Frank, R. (2009). Axisymmetric finite element analysis of pile loading tests. *Computers and Geotechnics*, 36(1-2), 6-19. http://dx.doi.org/10.1016/j.compgeo.2008.02.011.

Schanz, T., Vermeer, P.A., & Bonnier, P.G. (1999). The hardening soil model: formulation and verification. In *International Symposium Beyond 2000 in Computational Geotechnics* (pp. 281-296). Amsterdam: Routledge.

Schmidt, B. (1966). Discussion on: earth pressure at rest related to stress history. *Canadian Geotechnical Journal*, 3(4), 239-242. http://dx.doi.org/10.1139/t66-028.

Schmüdderich, C., Shahrabi, M.M., Taiebat, M., & Lavasan, A.A. (2020). Strategies for numerical simulation of cast-in-place piles under axial loading. *Computers and Geotechnics*, 125, 103656. http://dx.doi.org/10.1016/j.compgeo.2020.103656.

Tehrani, F.S., Nguyen, P., Brinkgreve, R.B.J., & van Tol, A.F. (2016). Comparison of press-replace method and material point method for analysis of jacked piles. *Computers and Geotechnics*, 78, 38-53. http://dx.doi.org/10.1016/j.compgeo.2016.04.017.

Teixeira, A.H., & Godoy, N.S. (1998). Análise, projeto e execução de fundações rasas. In Hachich, W., Falconi, F.F., Saes, J.L., Frota, R.G.Q., Carvalho, C.S., & Niyama, S. (Eds.), *Fundações: teoria e prática* (pp. 227-264). Pini. (in Portuguese).

Tovar-Valencia, R.D., Galvis-Castro, A., Salgado, R., & Prezzi, M. (2018). Effect of surface roughness on the shaft resistance of displacement model piles in sand. *Journal of Geotechnical and Geoenvironmental Engineering*, 144(3), 04017120. http://dx.doi.org/10.1061/(asce)gt.1943-5606.0001828.

Wehnert, M., & Vermeer, P.A. (2004). Numerical analyses of load tests on bored piles. In *9th International Symposium on Numerical Models in Geomechanics* (pp. 505-511). Ottawa: CRC Press.

White, D.J., & Bolton, M.D. (2004). Displacement and strain paths during plane-strain model pile installation in sand. *Geotechnique*, 54(6), 375-397. http://dx.doi.org/10.1680/geot.54.6.375.45427.

White, D.J., & Lehane, B.M. (2004). Friction fatigue on displacement piles in sand. *Geotechnique*, 54(10), 645-658. http://dx.doi.org/10.1680/geot.2004.54.10.645.

Yang, Z.X., Gao, Y.Y., Jardine, R.J., Guo, W.B., & Wang, D. (2020). Large deformation finite-element simulation of displacement-pile installation experiments in sand. *Journal of Geotechnical and Geoenvironmental Engineering*, 146(6), 04020044.